https://doi.org/10.22226/2410-3535-2022-2-111-115

Molecular dynamics study of the influence of free volume and orientation of the crystallization front on its velocity in nickel

G. M. Poletaev[†,1], I. V. Karakulova[1], D. V. Novoselova[2], R. Y. Rakitin[3]

[†]gmpoletaev@mail.ru

[1]Polzunov Altai State Technical University, Barnaul, 656038, Russia
[2]Kuzbass Institute of the Federal Penitentiary Service of Russia, Novokuznetsk, 654066, Russia
[3]Altai State University, Barnaul, 656049, Russia

The influence of free volume and orientation of the crystallization front relative to the growing crystal on the velocity of the front movement in nickel was studied by the method of molecular dynamics. The computational cells had the shape of elongated parallelepipeds, at the ends of which the crystal structure was fixed, that imitated the starting position of the heterogeneous crystallization front. Three different orientations of the front relative to the growing crystal were considered: (100), (110), and (111). The concentration of the excess free volume and the formation of vacancy clusters occurred mainly in last turn, at the final stage of crystallization. The introduction of excess free volume led to a decrease in the crystallization velocity. At high concentrations of several percent, the formation of some clusters occurred already at the early stages of crystal growth, but most of them, nevertheless, were located at the meeting point of two fronts from different ends of the computational cell. Crystallization proceeded faster at the (100) front orientation, slower at the (110) and (111) orientations. The anisotropy of the crystallization velocity is related to the difference between the free energies of an atom near the boundary in the liquid phase and a growing crystal «imbedded» into the boundary, which depends on the orientation of the boundary and, in particular, correlates with the energy of the adatom on the corresponding free surface of the crystal.

Keywords: molecular dynamics, crystallization, metal, free volume.

1. Introduction

Solidification and the accompanying crystallization of metals and alloys are technologically widespread and important processes that have a significant impact on the final structure of the material. Despite the great attention to the crystallization process and its long-term study, there are still unresolved questions even for pure metals, and this applies not only to the kinetics of a relatively more complex homogeneous crystallization mechanism [1,2] associated with the nucleation of crystalline nuclei, but also heterogeneous [3–7], when the process is accompanied by the movement of the crystallization front. In particular, at present there are two competing kinetic models of the motion of the crystallization front: with limitation of thermal collisions of atoms (collision limited) and with diffusion limitation (diffusion limited) [1,3,6]. Due to the impossibility of carrying out appropriate experiments at superhigh undercooling temperatures, which, as a rule, did not exceed 20% of the melting temperature [8,9], it was long believed that the rate of solidification in its pure form is controlled by kinetics limited by collisions of atoms [10–12]. However, it was assumed that there is no energy barrier for the motion of an atom through the liquid-crystal boundary. Later, when it became possible to conduct experiments with deep undercooling (for example, in [6] silver was undercooled up to 40% of the melting temperature), it was shown that this model disagrees with the experiment in the region of high undercooling temperatures. According to this model, as the temperature decreases, the crystallization rate should increase monotonically, however, in reality, as the experiment showed [6], this growth stops approximately at $0.6-0.8\cdot T_m$, and with a subsequent decrease in temperature, the rate even slightly decreases, which is well explained by the diffusion-limited model, which takes into account the decrease in the diffusion mobility of atoms in the amorphous phase with decreasing temperature.

Another important feature of the kinetics of the crystallization front is the anisotropy of its velocity. In [4,7,13–15], using computer simulation, it was found that the velocity of the liquid-crystal boundary depends on its orientation relative to the crystal. In particular, it was shown in the works mentioned that the boundaries oriented along the (100) plane move faster than others in fcc metals.

This work is devoted to the study of the influence of free volume, which can form in the melt, for example, as a result of crystallization from different centres [16,17], and orientation of the crystallization front relative to the growing fcc crystal on the front velocity in nickel. Three front orientations were considered: (100), (110) and (111). Nickel was chosen as a typical fcc metal, for which a fairly large set of experimental data has been collected, and there are well-tested interatomic interaction potentials.

2. Description of the model

Modelling was carried out using computational cell in the form of an elongated parallelepiped with a square cross section (Fig. 1). The computational cell contained 100–120 thousands atoms, was about 5.8 nm high and wide, and 37.5 nm long. At the ends of the parallelepiped (along *z* axis), the crystal structure was fixed (dark gray atoms in Fig. 1), which imitated the starting position of the crystallization front. Along another axes, *x* and *y*, periodic boundary conditions were imposed.

To describe interatomic interactions in nickel, the many-particle potentials of Cleri and Rosato [18] were used. Potentials of this type have been repeatedly used in molecular dynamics models and have been tested for a large number of characteristics [19–21]. The experience of their application shows that with their help it is possible to describe the various properties of metals and alloys. The time integration step in the molecular dynamics method was 2 fs. The temperature in the model was set through the initial velocities of the atoms according to the Maxwell-Boltzmann distribution, taking into account the thermal expansion of the computational cells. To keep the temperature constant during the simulation, a Nose-Hoover thermostat was used.

At the first stage, the computational cell was melted by holding it at a temperature significantly higher than the melting point (Fig. 1 shows a melted cell). Then the thermostat was turned on, and holding was carried out at a given constant temperature. During the molecular dynamics experiment, the crystallization front moved from the ends of the computational cell to its centre.

The free volume was introduced into the model at the initial stage by setting a certain concentration of vacancies. In the main computer experiments, the volume of the computational cell after setting the temperature remained constant, which made it possible to clearly estimate the value of the free volume in the cell. The concentration of vacancies introduced into the computational cell at the initial stage of simulation varied in a wide range from 0 to 7%. The latter value exceeds the equilibrium concentration of vacancies by more than two orders of magnitude, but at the same time, this allows us to consider the effect of vacancy clusters that arise, for example, during radiation damage, the presence of pores, on the crystallization process.

The melting temperature of nickel in the model under consideration (1750 K) agreed quite well with the reference value (1726 K). The potential used also quite accurately describes the thermal expansion: the value of the coefficient of linear thermal expansion obtained by the model is $1.42 \cdot 10^{-5}$ K^{-1}, which is close to the reference value of $1.50 \cdot 10^{-5}$ K^{-1} [18]. When setting one or another constant temperature, the thermal expansion of the computational cell was taken into account, but with respect to an ideal crystal. The consequence of this was the presence at the initial stage in the liquid metal of additional internal pressure due to the difference in the densities of the liquid and crystalline states, which corresponded approximately to a deformation of 1.3% (the atomic volume in the model for the crystalline state at a temperature of 1750 K was 11.77 Å^3, for the melt –12.24 Å^3). However, on the other hand, in this case it was possible to clearly estimate the amount of excess volume after the completion of crystallization. In addition, the introduction of a high concentration of vacancies on the order of several percent into the starting cell led to the formation of a negative pressure even in molten nickel.

3. Results and discussion

Front velocity was determined as the average speed of the left and right fronts:

$$\upsilon = \frac{\Delta l_1 + \Delta l_2}{2\Delta t}, \qquad (1)$$

where Δl_1 and Δl_2 are distances travelled by the crystallization front in the upper and lower parts of the computational cell during the time Δt (Fig. 2). In most cases, the position of the front was clearly visible visually. The determination error did not exceed, as a rule, two atomic planes.

Fig. 3 shows the temperature dependences of the crystallization velocity obtained in this work for three different orientations of the front relatively growing fcc crystal: (100), (110) and (111). According to the data obtained, the crystallization velocity with an increase in the undercooling temperature does not increase monotonically, but has a maximum at 0.7 of the melting point, after which it gradually decreases.

Such behaviour in the region of super-high values of undercooling is well described by the Wilson-Frenkel model with diffusion limitation [1, 3, 5, 6]:

$$\upsilon(T) = A \exp\left(-\frac{E}{kT}\right)\left[1 - \exp\left(-\frac{\Delta\mu}{kT}\right)\right]. \qquad (2)$$

Here A is the preexponential factor, E is the activation energy of the migration of an atom in the liquid phase, k is the Boltzmann constant, T is the temperature, $\Delta\mu$ is the difference between the free energies of the liquid and crystalline states.

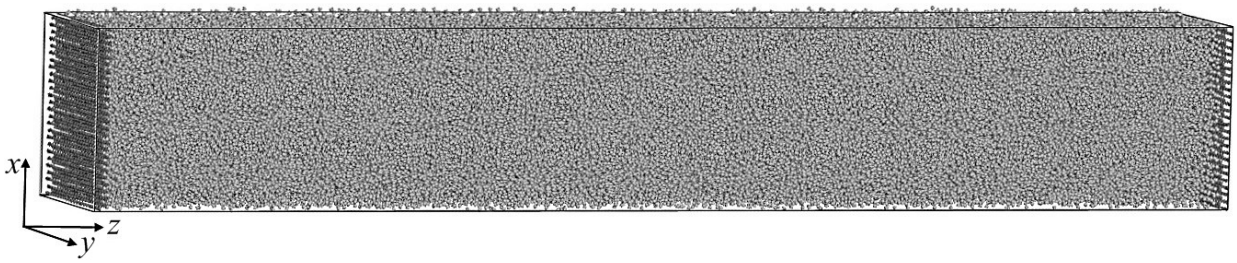

Fig. 1. Computational cell for modeling crystallization (dark gray atoms at the ends of the cell remained motionless during the simulation).

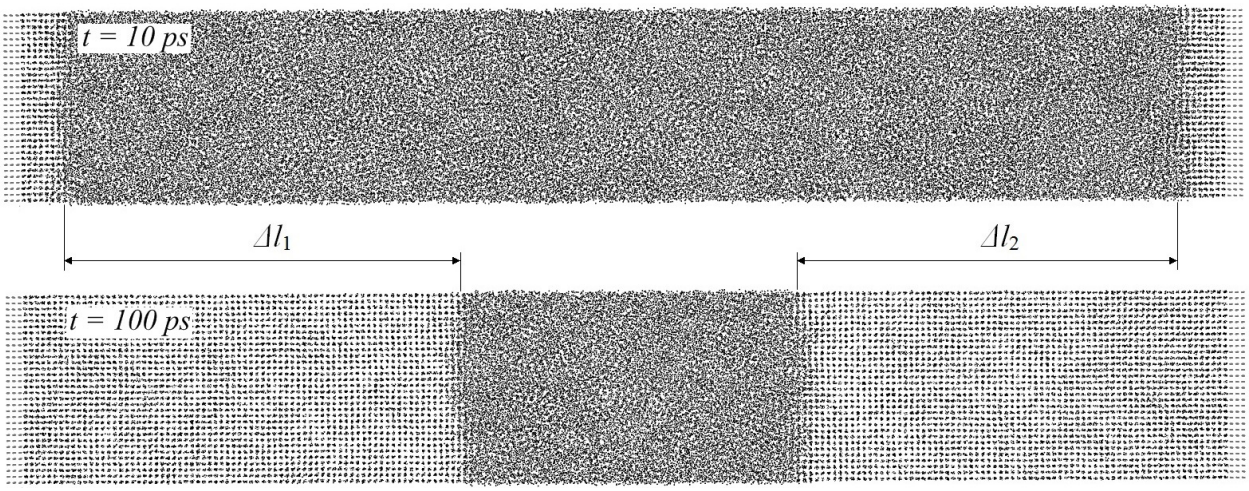

Fig. 2. To the method of calculating the velocity of the crystallization front movement.

In our case, the main factor responsible for the effect of temperature on the velocity of the crystallization front is the value of E in formula (2), i. e. diffusion mobility of atoms in the amorphous phase. With a decrease in temperature, this mobility decreases exponentially, and at a certain temperature (at $0.7 \cdot T_m$ in our case), this decreasing contribution begins to prevail over the increasing contribution of the second factor in formula (2).

As can be seen from Fig. 2, crystallization proceeds faster with the front orientation (100), slower — with the (110) and (111) orientations. To explain the anisotropy of the crystallization velocity, one should obviously pay attention to the second factor in formula (2) and the value of Δμ, which is usually defined as the difference between the free energies of the liquid and crystalline states. However, near the liquid-crystal interface, it is not the difference in energies within the volumes of the crystal and the liquid is of greater importance, but the difference in the free energies of an atom near the interface in the liquid phase and of an atom "imbedded" into the boundary of a growing crystal. If the value of Δμ is determined in this way, it ceases to be constant and becomes dependent on the orientation of the liquid-crystal interface. This energy can be compared with the energy of an adatom on the corresponding free surface of the crystal, or with the activation energy of its migration over a given surface. For example, in [22], the activation energies of surface self-diffusion were obtained for nickel: 0.33 eV over the free (111) surface and 0.63 eV over the (100) surface.

To confirm this assumption, we separately have found the values of the potential energy of Ni atom on (111) and (100) surfaces of nickel crystal: −2.67 and −2.85 eV, respectively. In addition, the energies of the atom near the monatomic step on the surfaces under consideration were found: −3.16 and −3.34 eV, respectively. In both cases, as can be seen, the potential well in which the adatoms are located is deeper in the case of the (100) surface compared to the well on the (111) surface, which is the main reason for the difference in the velocities of the crystallization front for the (111) and (100) orientations.

The maximum values of the crystallization velocity obtained in our work at $0.7 \cdot T_m$ coincide with the values given in [7] for nickel, where they were obtained by modelling using another potential: 150 m/s for (100) orientation and 100 m/s for (110) orientation.

Fig. 4 shows the dependences of the crystallization velocity on the concentration of vacancies introduced at the initial stage at a thermostat temperature of 1300 K (which is

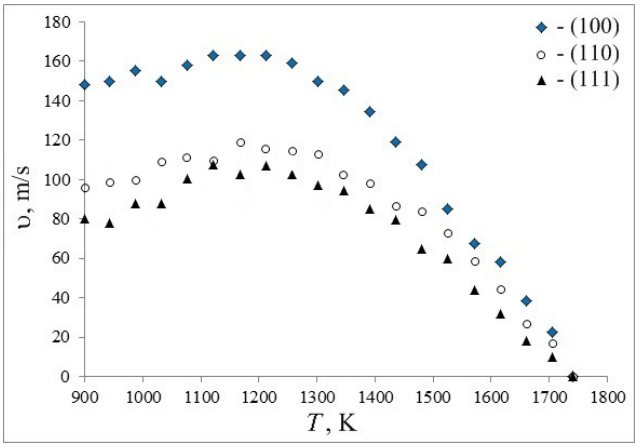

Fig. 3. (Color online) Dependences of the crystallization front velocity on the temperature for three different front orientations.

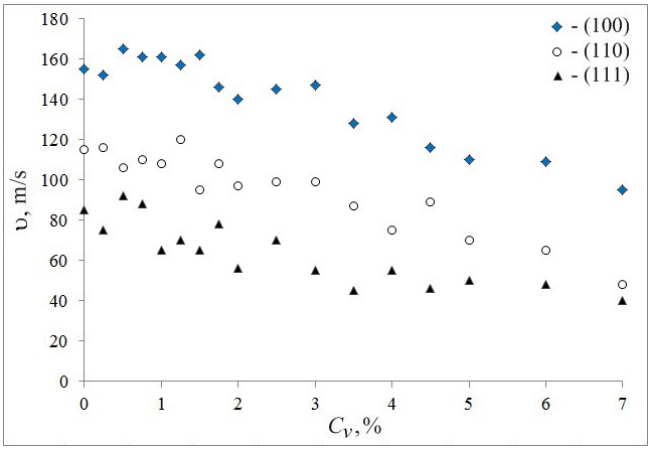

Fig. 4. (Color online) Dependences of the velocity of the crystallization front on the concentration of vacancies introduced at the initial stage at a temperature of 1300 K for the three considered front orientations: (100), (110), and (111).

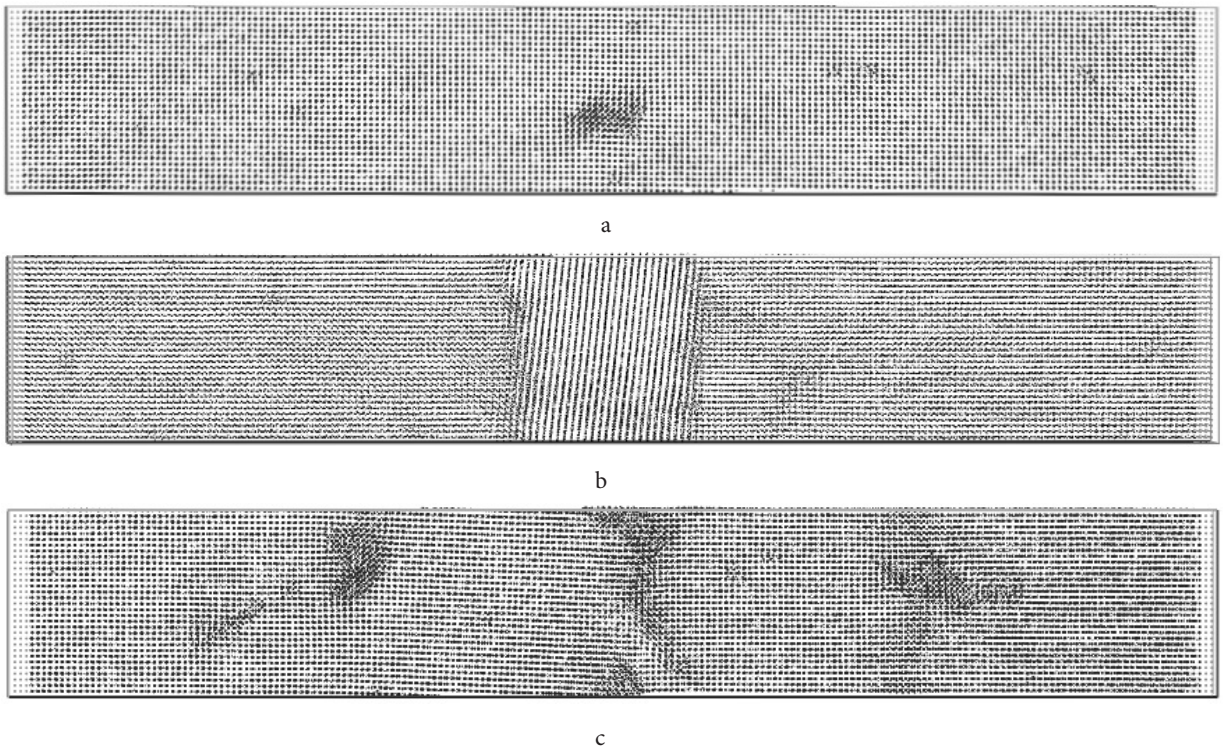

Fig. 5. Concentration of excess free volume during crystallization at front orientation (100) at concentration of vacancies introduced at the initial stage: 1.25% (a); 4.5% (b); 6% (c).

$0.75 \cdot T_m$) obtained in this work for three front orientations: (100), (110) and (111). The introduction of excess free volume, as can be seen from Fig. 4, reduces the velocity of crystallization. This is an unobvious result, since the activation energy of self-diffusion E with an increase in the free volume, in this case, should decrease, and, according to the Wilson-Frenkel model (2), the velocity of the front, therefore, should increase. But the opposite result is observed. Apparently, this phenomenon can be explained by the formation of micropores and vacancy clusters near the growing crystal boundary, which generally reduce the access of atoms from the liquid phase to the crystal boundary. In addition, as mentioned in the second section, one should take into account the presence in the computational cell of internal pressure due to the difference in the densities of liquid and crystalline nickel, which decreases as the metal crystallizes. This pressure also decreases with the introduction of vacancies at the initial stage and even becomes negative at sufficiently high vacancy concentrations.

The concentration of the excess free volume and the formation of vacancy clusters occurred mainly last, at the final stage of crystallization. At relatively low concentrations of vacancies introduced at the initial stage, the growing crystal did not contain defects; vacancy clusters formed, as a rule, at the very end, when the right and left fronts met (Fig. 5a). With increasing concentration, it was sometimes not the formation of vacancy clusters that was energetically favourable, but the formation of grain boundaries, as, for example, in Fig. 5b. However, at high concentrations of several percent, some of the clusters formed already at the early stages of crystal growth (Fig. 5c), but most of them, nevertheless, were located at the meeting point of two fronts from different ends of the computational cell.

4. Conclusion

The influence of free volume and orientation of the crystallization front relative to the growing crystal on the front velocity in nickel was studied by the method of molecular dynamics. The concentration of the excess free volume and the formation of vacancy clusters occurred mainly last, at the final stage of crystallization. The introduction of excess free volume led to a decrease in the crystallization velocity. At high concentrations of several percent, the formation of some clusters occurred already at the early stages of crystal growth, but most of them, nevertheless, were located at the meeting point of two fronts from different ends of the computational cell.

Crystallization proceeded faster at the (100) front orientation, slower at the (110) and (111) orientations. The anisotropy of the crystallization velocity is related to the difference between the free energies of an atom near the boundary in the liquid phase and a growing crystal "imbedded" into the boundary, which depends on the orientation of the boundary and, in particular, correlates with the energy of the adatom on the corresponding free surface of the crystal.

References

1. P.K. Galenko, V. Ankudinov, K. Reuther, M. Rettenmayr, A. Salhoumi, E.V. Kharanzhevskiy. Philosophical Transactions of the Royal Society A: Mathematical, Physical and Engineering Sciences. 377, 20180205 (2019). Crossref
2. S.K. Jha, S. Karthika, T.K. Radhakrishnan. Resource-Efficient Technologies. 3, 94 (2017). Crossref

3. V.I. Mazhukin, A.V. Shapranov, V.E. Perezhigin, O.N. Koroleva, A.V. Mazhukin. Mathematical Models and Computer Simulations. 9, 448 (2017). Crossref
4. M.I. Mendelev, F. Zhang, H. Song, Y. Sun, C.Z. Wang, K.M. Ho. The Journal of Chemical Physics. 148, 214705 (2018). Crossref
5. G. Sun, J. Xu, P. Harrowell. Nature Materials. 17, 881 (2018). Crossref
6. W.-L. Chan, R.S. Averback, D.G. Cahill, Y. Ashkenazy. Physical Review Letters. 102, 095701 (2009). Crossref
7. H.Y. Zhang, F. Liu, Y. Yang, D.Y. Sun. Scientific Reports. 7, 10241 (2017). Crossref
8. D. Turnbull, R.E. Cech. Journal of Applied Physics. 21, 804 (1950). Crossref
9. K.K. Leung, C.P. Chiu, H.W. Kui. Scripta Metallurgica et Materialia. 32, 1559 (1995). Crossref
10. C.A. MacDonald, A.M. Malvezzi, F. Spaepen. Journal of Applied Physics. 65, 129 (1989). Crossref
11. S.R. Coriell, D. Turnbull. Acta Metallurgica. 30, 2135 (1982). Crossref
12. J.Q. Broughton, G.H. Gilmer, K.A. Jackson. Physical Review Letters. 49, 1496 (1982). Crossref
13. M.I. Mendelev, M.J. Rahman, J.J. Hoyt, M. Asta. Modelling and Simulation in Materials Science and Engineering. 18, 074002 (2010). Crossref
14. J.J. Hoyt, M. Asta, A. Karma. Interface Science. 10, 181 (2002). Crossref
15. D.Y. Sun, M. Asta, J.J. Hoyt. Physical Review B. 69, 024108 (2004). Crossref
16. G.M. Poletaev, D.V. Novoselova, I.V. Zorya, M.D. Starostenkov. Physics of the Solid State. 60, 847 (2018). Crossref
17. G.M. Poletaev, D.V. Novoselova, R.Y. Rakitin, A.S. Semenov. Letters on Materials. 10 (3), 299 (2020). Crossref
18. F. Cleri, V. Rosato. Physical Review B. 48, 22 (1993). Crossref
19. C. Chen, F. Zhang, H. Xu, Z. Yang, G.M. Poletaev. Journal of Materials Science. 57, 1833 (2022). Crossref
20. G.M. Poletaev, I.V. Zorya, R.Y. Rakitin, M.A. Iliina. Materials Physics and Mechanics. 42, 380 (2019). Crossref
21. R.Y. Rakitin, G.M. Poletaev, M.S. Aksenov, M.D. Starostenkov. Technical Physics Letters. 31, 650 (2005). Crossref
22. C.L. Liu, J.M. Cohen, J.B. Adams, A.F. Voter. Surface Science. 253, 334 (1991). Crossref